Reports

Volcanic Eruptions: Contribution to Magnetism in Deep-Sea Sediments Downwind from the Azores

Abstract. *The mean bulk magnetic susceptibility ($\bar{\chi}$) and the intensity of remanent magnetization ($\bar{J}$) of deep-sea sediments vary systematically, but in an opposite sense, for a distance of 600 kilometers downwind from the Azores. Beyond the distance both $\bar{J}$ and $\bar{\chi}$ diminish for at least another 600 kilometers. The dominant type of magnetic particle in the sediments is interpreted to be atmospherically transported volcanic dust.*

Until the history of geomagnetic reversals had been established with the use of the potassium-argon method and paleomagnetic studies of lavas (*1*), with only rare exceptions (*2*) the magnetic properties of deep-sea sediments were ignored. The emergence of the polarity time scale (*3*) provided the opportunity to overcome critical dating problems in deep-sea sediments (*4*). Paleomagnetic methods are now becoming conventional means of recognizing isochrons in Pliocene and Pleistocene sediment cores (*3, 5*) although some possible dynamic (*6*) and chemical (*7*) distortions of the paleomagnetic signature are suspected.

Despite substantial present-day application of the paleomagnetic dating technique to deep-sea sediments, the source of magnetism in deep-sea sediments is still poorly understood. Although thermomagnetic and x-ray diffraction methods have recently been used to identify the mineralogy of various extracts from deep-sea sediments (*8*), such methods cannot resolve the problem of whether the paleomagnetic properties of samples 10 cm^3 or larger are in fact unambiguously due to the effect of the separates examined, which may not necessarily be dominant contributors to the net directions of the remanent magnetism. As Kent and Lowrie stress (*9*), diagnosis of the mineralogy of the very fine (< 1 μm) magnetic particles is very difficult, and it is these particles which may be of the greatest magnetic significance. Similarly, identification of magnetic minerals by optical techniques (*10*) is limited by the resolving power (10 μm or so) of available reflection microscopes, so that, although high-temperature titanomagnetite phases can be recognized in detrital particles present, the bulk paleomagnetic properties need not necessarily mirror those of the restricted observed components. In all such approaches to an understanding of the mineralogy of the magnetic fraction the inherent heterogeneity of associated sources of such particles in deep-sea sediments must be taken into account: unlike basalts, which almost invariably have a relatively limited range of magnetic mineralogy and a common thermal history no matter what age or geographic province is involved, the particles comprising deep-sea sediments are fine enough to be atmospherically transported. This does not exclude the possibility of authigenic production of magnetic minerals on the sea floor or detrital contributions from submarine sources. Therefore, over a long period, deep-sea sediments may be very diverse in fine particle composition. In order to understand the dominant magnetic mineralogy of sediments, it therefore becomes necessary to develop means to analyze the bulk properties, preferably with the use of techniques which can make it possible to identify the parent source of magnetic particles which are likely to be as fine as 1 μm or less.

Cruise 121 of R.V. *Trident* in August 1972 was designed in part to provide a collection of deep-sea sedimentary cores with a distribution such that suspected source regions for magnetic minerals could be recognized. All the cores of 6-cm diameter were taken in plastic liners. Figure 1 shows the locations of 13 cores taken in a traverse extending 1200 km downwind from the Azores, which are entirely volcanic (*11*). The major part of the exposed volcanic deposits and lavas on the islands are of Pleistocene age. The exact core lengths, locations, and water depths are given in Table 1. The sediment in the suite of cores has been described by Corliss (*12*) and Huang *et al.* (*13*) as being mainly foraminiferal ooze. Up to nine megascopically distinguishable ash horizons are intercalated with the upper 10 m of sediments in the cores near the islands, but this number decreases rapidly eastward. Conventional separation of the coarse fractions and binocular microscope examinations show that there are four types of volcanic

Scoreboard for Reports: In the past few weeks the editors have received an average of 57 Reports per week and have accepted 12 (21 percent). We plan to accept about 10 reports per week for the next several weeks. In the selection of papers to be published we must deal with several factors: the number of good papers submitted, the number of accepted papers that have not yet been published, the balance of subjects, and length of individual papers.

Authors of Reports published in *Science* find that their results receive good attention from an interdisciplinary audience. Most contributors send us excellent papers that meet high scientific standards. We seek to publish papers on a wide range of subjects, but financial limitations restrict the number of Reports published to about 12 per week. Certain fields are overrepresented. In order to achieve better balance of content, the acceptance rate of items dealing with physical science will be greater than average.

Table 1. Mean magnetic susceptibility ($\bar{\chi}$) and intensity of magnetization ($\bar{J}$) of deep-sea sedimentary cores downwind from the Azores. The core number represents the number of the core in order of collection during *Trident* cruise 121; the core length is the length of the upper 150,000-year core segment; $\bar{\chi}$ in centimeter-gram-second units $\times 10^6$; $\sigma\bar{\chi}$ = standard deviation of $\bar{\chi}$; $\bar{J}$ in electromagnetic units per cubic centimeter $\times 10^6$; $\sigma\bar{J}$ = standard deviation of $\bar{J}$.

	Location								
Core No.	Latitude (°N)	Longitude (°W)	Water depth (m)	Core length (m)	Data points (No.)	$\bar{\chi}$	$\sigma\bar{\chi}$	$\bar{J}$	$\sigma\bar{J}$
2	38.47	26.38	1700	3.30	33	44	4.45	5.5	0.06
6	38.79	23.99	3770	3.90	39	34	6.77	8.8	0.78
10	39.30	20.57	5090	3.00	29	19	5.02	10.0	1.54
12	39.55	19.33	5250	2.50	18	11	4.17	5.1	0.42
13	39.65	18.71	4820	2.00	20	17	0.71	2.9	0.77
15	38.95	17.98	5225	1.70	17	13	0.29	5.0	1.20
17	38.40	20.03	4775	2.90	28	22	4.50	11.0	1.98
18	38.40	20.58	4900	2.70	26	14	0.74	11.1	1.34
19	38.26	21.30	4700	3.40	33	30	16.07	14.5	4.04
21	38.17	22.28	4500	3.30	32	31	12.0	13.8	4.00
26	37.89	23.85	3500	3.00	29	38	7.9	17.0	2.42
30	38.33	25.31	2875	3.10	30	57	12.96	7.6	2.25

particles present: basaltic vesicular shards, basaltic vitreous glass, rhyolitic glass, and pumice (*13*). Prior to the splitting of each core, we measured the intensity of the remanent magnetism (J) and the relative declination of the natural remanent magnetism at core intervals of 2 to 6 cm, using a Digico spinner magnetometer (*14*) with a long-core attachment (*15*). After this, a low-field susceptibility bridge with a pull-through system (*16*) was used to measure the magnetic susceptibility (χ) at similar intervals along each core. Splitting the cores then facilitated conventional paleomagnetic and micropaleontological examination. All these cores had normal polarity throughout and are confined to the Brunhes epoch (0 to 0.69×10^6 years). Micropaleontological zonation (*12*) has yielded apparent sedimentation rates of between 1.1 and 2.5 cm per 1000 years for the cores.

An arbitrary age range of 0 to 150,000 years was chosen for examination of the magnetic properties. Use of a common isochron is clearly essential, since any between-core variations of J and χ could otherwise be meaningless. The mean and standard deviations of J and χ are given as $\bar{J}$ and $\bar{\chi}$ in Table 1. The data are plotted as a function of distance in Fig. 2. Least-squares residual regression lines have been added to Fig. 2. Conventional comparisons of the rate of decrease of the mean residual with increasing order of regression show that $\bar{\chi}$ best varies according to a first-order function and $\bar{J}$ according to a second-order function. Corresponding first- and second-order trend surfaces, based on $\bar{\chi}$ and $\bar{J}$ values, are shown in Fig. 1, a and b, respectively.

Figure 2 shows that χ is a clear first-order function of distance from the islands. The quantity χ is best considered as a simple measure of the bulk magnetic mineral content, independent of any preferred orientation of the magnetic particles involved. This is consistent with the interpretation that the material causing the variation is affected by processes which diminish with distance from the islands. The first-order trend surface map (Fig. 1a) also reflects this fact. By far the simplest of the possible mechanisms available that could be responsible for this observation of volcanic dust is atmospheric transport (which is highly magnetic) from the islands. The contours in Fig. 1a would then be oriented normal to the regional wind directions, which are in fact dominantly to the northeast. Any other mechanism, such as selective winnowing or authigenic alteration of magnetic particles on the sea floor as a function of distance from the islands, is unlikely. Similarly, systematic dilution of relatively unvarying magnetic particle accumulation by materials which increase in concentration away from the islands is untenable, since there is no variation in the net parallel sedimentation rate. The role of microorganisms in the great acceleration of particle deposition between the sea surface and sea bottom (relative to that which would occur for single particles) is now well known (*17*), so that lateral transport by currents can be essentially ignored (*18*).

Support for the hypothesis that the simple decrease of $\bar{\chi}$ with distance from the islands is caused by atmospherically transported volcanic dust comes from the observed variation of $\bar{J}$ (Fig. 2). In contrast with $\bar{\chi}$, values of $\bar{J}$ depend largely on the net alignment of the magnetic particles in the sediment. In order for an average magnetic sedimentary particle to be aligned by the geomagnetic field as opposed to the gravity field (and thus contribute to the natural remanent magnetism), its size, according to King and Rees (*19*), must not exceed 50 μm. Much smaller critical sizes are suggested by Kent and Lowrie (*9*). Thus one might expect $\bar{J}$ to increase with distance from the source, as the coarser particles (capable of only random orientation by gravity couples) diminish in concentration. Thus $\bar{J}$ would reach a maximum at the point where there exists a maximum concentration of fine (oriented) particles. We believe that our data in Fig. 2 reflect this fact. Beyond 600 km, $\bar{J}$ and $\bar{\chi}$ diminish in parallel, virtually linear fashion, which is to be expected if $\bar{\chi}$ expresses a simple diminishing concentration of fine magnetic particles, all of which, because of their fine size, tend to contribute to $\bar{J}$. At distances less than 600 km the magnetic particles increase in concentration (as $\bar{\chi}$) toward the source, but are of coarser size, so that $\bar{J}$ decreases toward the source. We propose that the only plausible explanation for these data (Fig. 2) is volcanic eruptions to substantial heights producing volumes of dust which are transported downwind. The trend surface map of $\bar{J}$ (Fig. 1b) suggests that finer materials may also be selectively transported southward, perhaps reflecting net wind directions that change with increasing altitude, which the finer materials may be expected to reach. The volcanic explosivity modeling of Shaw *et al.* (*20*), in which data from nuclear bomb

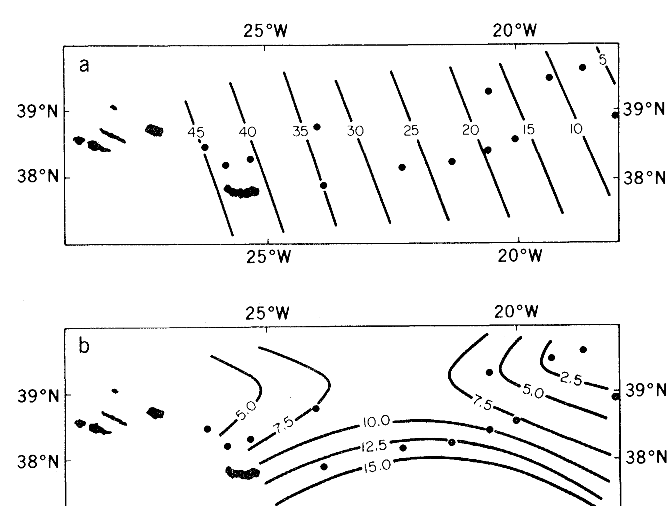

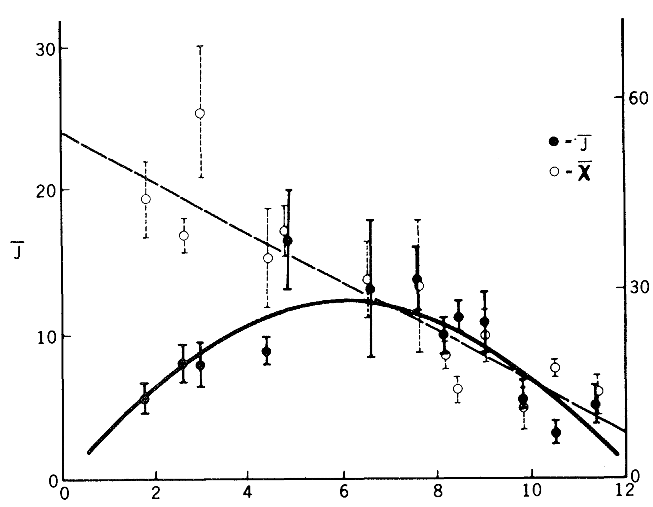

Fig. 1 (left). (a) Map showing the eastern part of the Azores Islands: core locations (dots) and contours of the first-order trend surface map of the mean magnetic volume susceptibility ($\bar{\chi}$) for each core. (b) Same as (a), with contours on a second-order trend surface for mean values of the intensity of magnetization ($\bar{J}$) for each core. The units of $\bar{J}$ and $\bar{\chi}$ are as in Table. 1. Fig. 2 (right). Relationship between the mean intensity of magnetization ($\bar{J}$), the mean magnetic volume susceptibility ($\bar{\chi}$), and the distance from San Jorge Island for the series of deep-sea sedimentary cores (Fig. 1). Error bars are 1 standard deviation; the units of $\bar{J}$ and $\bar{\chi}$ are the same as those given in Table 1. Least-squares residual lines have been added: a first-order line for $\bar{\chi}$ and a second-order line for $\bar{J}$.

tests are used (*21*), suggests that an average explosive volcanic cloud height of at least 7000 m would be involved to yield a dominant particle size of 50 μm or less at a distance of 600 km.

Preliminary results of detailed particle size analyses of the atmospherically transported volcanic dust and micropumice fragments in the cores are now available (*13*), and they support completely our inference of a downwind decrease in volcanic dust concentrations which, according to examination by binocular and transmitted light microscopy, are unaltered by any seafloor processes.

Windom's (*22*) proposal that deep-sea sediments may contain large fractions of windblown materials is supported by our data, which further suggest that one may map the contribution from suspected volcanic sources by measuring magnetic properties of cores from traverses or grids focused on the source region. Furthermore, such data can be rapidly obtained from cores in unsplit plastic liners.

W. KENNETH FREED
NORMAN D. WATKINS
Graduate School of Oceanography, University of Rhode Island, Kingston

References and Notes

1. A. Cox, R. R. Doell, by G. B. Dalrymple, *Science* **144**, 1537 (19 I. McDougall and F. H. Chamalaun, *Nature (Lond.)* **212**, 1415 (1966).
2. M. J. Keen, *Deep-Ses Res.* **10**, 607 (1963); C. G. A. Harrison, *J. Geophys. Res.* **71**, 3033 (1966).
3. Summarizec N. D. Watkins in *Geol. Soc. Am. Bull.* **83**, 551 (1972).
4. N. D. Opdyke, B. Glass, J. D. Hays, J. Foster, *Science* **154**, 349 (19 N. D. Watkins and H. G. Goodell, *Earth Planet. Sci. Lett.* **2**, 123 (1967).
5. N. D. Opdyke, *Rev. Geophys. Space Phys.* **10**, 213 (19 C. G. A. Harrison, *Earth-Sci. Rev.* **10**, 1 (1974).

C. Amerigian, *Earth Planet. Sci. Lett.* **21**, 321 (1974).

N. D. Watkins, D. R. Kester, J. P. Kennett, *ibid.* **24**, 113 (1974).

R. Løvlie, W. Lowrie, M. Jacobs, *ibid.* **15**, 157 (1971).

9. D. V. Kent and W. Lowrie, *J. Geophys. Res.* **79**, 2987 (1974).
10. S. E. Haggerty, *Carnegie Inst. Washington Yearb.* **68**, 332 (1970).
11. W. I. Ridley, N. D. Watkins, D. J. MacFarlane, in *The Ocean Basins and Margins*, A. E. M. Nairn and F. G. Stehli, Eds. (Plenum, New York, 1973), vol. 2, pp. 445–483. All distances in the present study are measured from San Jorge Island.
12. B. H. Corliss, thesis, University of Rhode Island (1973).
13. T.-C. Huang, W. K. Freed, B. H. Corliss, *Geol. Soc. Am. Abstr. Programs* **6**, 801 (1974).
14. L. Molyneux, *Geophys. J. R. Astron. Soc.* **24**, 429 (1971).
15. ———, R. Thompson, F. Oldfield, M. E. McCallan, *Nat. Phys. Sci.* **237**, 42 (1972).
16. Bison Instruments magnetic susceptibility system model 3200, modified for the measurement of long cores by means of a pull-through coil attachment.

T. J. Smayda, *Mar. Geol.* **11**, 105 (1971); J. W. Pierce and B. O. Myers, *Geol. Soc. Am. Abstr. Programs* **6**, 388 (1974).

18. T.-C. Huang, N. D. Watkins, D. M. Shaw, *Geol. Soc. Am. Bull.*, in press.
19. R. F. King and A. I. Rees, *J. Geophys. Res.* **71**, 561 (1966).
20. D. M. Shaw, N. D. Watkins, T.-C. Huang, *ibid.* **79**, 3087 (1974).

B. R. Morton, G. Taylor, J. S. Turner, *Proc. R. Soc. Ser. A Math. Phys. Sci.* **234**, 1 (1956).

H. L. Windom *Geol. Soc. Am. Bull.* **80**, 761 (1969).

23. This research is supported by NSF grants GA 28853 and DES 74-22347.

17 December 1974; revised 4 March 1975

Structure of Coat Proteins in Pf1 and fd Virions by Laser Raman Spectroscopy

Abstract. *Raman spectra of filamentous bacterial viruses are dominated by scattering from vibrations of the protein capsomers. The amino acid compositions of coat proteins in Pf1 and fd strains are recognized by their different side-chain vibrational frequencies. However, the conformationally sensitive amide frequencies indicate that Pf1 and fd coat proteins have the same α-helical secondary structures. Viral DNA backbones do not exhibit the A-type geometry.*

A molecular model of filamentous bacterial viruses has been proposed on the basis of low resolution x-ray diffraction data (*1, 2*). Since details of the structure at the atomic level cannot be resolved by the x-ray data, it is essential to support the model by other lines of evidence. Using laser Raman spectroscopy, we present here the results of a study of protein and nucleic acid secondary structures in these viruses.

The method depends on the ability to obtain by laser light scattering a vibrational spectrum, consisting of a series of lines or frequencies characteristic of the structure and environment of macromolecular subgroups (*3*). Applications to nucleic acids (*4*) utilize the dependence of Raman frequencies and intensities on the amount and kind of base and backbone interactions to quantify RNA (*5*) and DNA (*6*) secondary structures. Applications to proteins (*7*) make use of the conformationally sensitive amide frequencies to distinguish α, β, and random-chain regions of the polypeptide backbone. Raman spectroscopy may also be applied to more complex assemblies, such as virions, to investigate stabilizing interactions of nucleic acid and protein (*8*). Information of high structural specificity is usually difficult to obtain on such systems by other techniques, particularly when water is used as a solvent.

We report here the Raman spectra of aqueous solutions of the filamentous bacterial (FB) viruses, Pf1 and fd strains. These are the first Raman spectra obtained on true DNA-protein complexes and are unusual for their high signal-to-noise quality and rich patterns of Raman lines.

The FB viruses are of considerable interest (*2*). Both Pf1 and fd are linear assemblies (19,500 Å and 9,000 Å, respectively, in length by 60 Å in diameter) of coat protein subunits encapsulating a DNA molecule. The DNA, which comprises not more than 12 percent by weight of either virion, is believed to be a circular single strand. The major coat protein in both strains comprises about 99 percent of all the viral protein, has a molecular weight of about 5000, and is believed to be largely α-helical in structure (*1, 2*). Primary structures of the major coat proteins in Pf1 and fd are, however, different (*1, 2, 9*). Proline, tryptophan, glutamic acid, and phenylalanine are absent from Pf1 but are present in fd, while glutamine and arginine are present in Pf1 but absent from fd.

Pf1 and fd were obtained and purified as described (*10*). For Raman spectroscopy solutions were prepared in 0.05*M* NaCl at *p*H 9. Spectra were excited with 488.0- and 514.5-nm lines of an argon-ion laser (Coherent Radiation Laboratories) and were recorded on a Ramalog spectrometer (Spex Industries, Inc.). Samples were contained in 1.0-mm capillary tubes and held at constant temperature as described (*11*).

All spectra were reproducible over a period of 48 hours, and changes in the spectra as a function of temperature were reversible over the range 32° to 75°C. Assays showed no loss of viral activity due to laser illumination or other sample handling.

The Raman data as recorded are shown in Fig. 1. Unusually high signal-to-noise ratios were obtained with both Pf1 and fd despite the noticeable background fluorescence in the latter case. The fluorescence is attributed to a viral component and not to impurities in the fd preparation. The spectra of both Pf1 and fd are dominated by Raman scattering of the coat protein in the regions 200 to 1800 cm^{-1} and 2800 to 3100 cm^{-1}.

Recent Raman studies of aqueous proteins and polypeptides (*7, 12, 13*) indicate the following. Helical structures give a strong and sharp amide I line at 1650 ± 5 cm^{-1} and relatively weak scattering in the amide III region (1265 to 1300 cm^{-1}). β-Structures give a strong and sharp amide I line at 1665 ± 5 cm^{-1} and a strong amide III line at 1235 ± 10 cm^{-1}. Random structures give a strong but broad amide I line at about 1665 cm^{-1} and a medium amide III line at 1248 ± 5 cm^{-1}. Therefore, the amide frequencies and intensities in Fig. 1 confirm that the coat proteins of Pf1 and fd have the same α-helical secondary structures. Furthermore, the absence of additional Raman scattering in the amide I region, which could be assigned to β or random structures, indicates that the coat proteins are uniformly α-helical (*14*). Weak Raman scattering near 1685 cm^{-1} in the spectra of Fig. 1 is attributed to the carbonyl stretching vibrations of the DNA bases (*3–6*).